Proceedings of the 6th European VLBI Network Symposium
Ros, E., Porcas, R.W., Lobanov, A.P., & Zensus, J.A. (eds.)
June 25th-28th 2002, Bonn, Germany

Higher Resolution VLBI Imaging with Fast Frequency Switching

E. Middelberg[1], A. L. Roy[1], R. C. Walker[2], H. Falcke[1], and T. P. Krichbaum[1]

[1] Max-Planck-Institut für Radioastronomie, Auf dem Hügel 69, 53121 Bonn, Germany
[2] National Radio Astronomy Observatory, P.O. Box 0, Socorro, NM 87801, USA

Abstract. Millimetre-VLBI is an important tool in AGN astrophysics, but it is limited by short atmospheric coherence times and poor receiver and antenna performance. We demonstrate a new kind of phase referencing for the VLBA, enabling us to increase the sensitivity in mm-VLBI by an order of magnitude. If a source is observed in short cycles between the target frequency, $\nu_{\rm t}$, and a reference frequency, $\nu_{\rm ref}$, the $\nu_{\rm t}$ data can be calibrated using scaled-up phase solutions from self-calibration at $\nu_{\rm ref}$. We have demonstrated the phase transfer on 3C 279, where we were able to make an 86 GHz image with 90 % coherence compared to self-calibration at $\nu_{\rm t}$. We have detected M81, our science target in this project, at 86 GHz using the same technique. We describe scheduling strategy and data reduction. The main impacts of fast frequency switching are the ability to image some of the nearest, but relatively weak AGN cores with unprecedented high angular resolution and to phase-reference the $\nu_{\rm t}$ data to the $\nu_{\rm ref}$ core position, enabling the detection of possible core shifts in jets due to optical depth effects. This ability will yield important constraints on jet properties and might be able to discriminate between the two competing emission models of Blandford-Königl jets and spherical advection-dominated accretion flows (ADAFs) in low-luminosity AGNs.

1. Introduction

The regions where AGN jets are launched and collimated are difficult to observe with VLBI because the jets are launched very close to the black hole and most of the bright objects are very distant. Only in the closest AGN in Sgr A*, M87, M84, Cen A and M81 can the highest resolution observations resolve several tens of Schwarzschild radii, comparable to the scale of 10-1000 $R_{\rm s}$ where jets are predicted to be launched and collimated (e.g. Koide et al. 2000, Appl & Camenzind 1993). Whilst the collimation regions remain unresolved in Sgr A* and M81, there are hints for resolving it in M87 (Junor et al. 1999).

The highest resolution VLBI images are currently achieved from observations at 86 GHz. However, short atmospheric coherence times and poor receiver performance and antenna efficiencies severely limit the observations to sources with $S_{86\,\rm GHz} \sim 0.4$ Jy. We have developed a new phase-referencing strategy for the VLBA that is not limited by self-calibration at the target frequency $\nu_{\rm t}$, but only at a lower reference frequency $\nu_{\rm ref}$. A source is observed switching between these two frequencies on a timescale that does not exceed half the atmospheric coherence time. After self-calibrating the $\nu_{\rm ref}$ data, the phase solutions are multiplied by the frequency ratio $r = \nu_{\rm t}/\nu_{\rm ref}$ and added to an instrumental, antenna-based phase offset $\Delta\phi$. Using these phases, the $\nu_{\rm t}$ data can be imaged.

In a pilot project, we have observed M81 and 3C 279 on January 5, 2002, with various frequency pairs and cycle times to develop the calibration technique. We describe the details and results of this project and what we have learnt for future observations.

2. Observing Strategy and Frequencies

The Very Long Baseline Array offers the opportunity to switch between frequencies in less than ten seconds. Frequency switching is done by moving the sub-reflector, and therefore the switching time is limited by its speed (the setup of the electronics only takes one or two seconds). The frequency selection is governed by three considerations. 1) The feed horns should lie as close as possible on the antenna feed circle in the secondary focus to minimise the switching times and hence the data loss. 2) The phase noise at $\nu_{\rm t}$ should be as low as possible, and one should therefore select $\nu_{\rm ref}$ such that the combination of antenna performance (antenna efficiency and receiver noise) and source flux density at $\nu_{\rm ref}$ yields little phase noise after multiplication by r. 3) The target source needs to be strong enough for self-calibration during the envisaged integration time at $\nu_{\rm ref}$. One should at least expect a 5 σ detection within this integration time.

We assumed a nominal coherence time at 86 GHz of 30 s when planning the experiment and therefore selected an integration time of 15 s per frequency. We expected a data loss of 5 s due to frequency switching, leaving 10 s of data at each frequency. Within 10 s, and using 256 Mbps recording for higher sensitivity, we calculated the theoretical SNRs for three potential reference frequencies 15 GHz, 22 GHz and 43 GHz (Table 1). However, the 22 GHz feed horn has a large angular separation from the 86 GHz feed horn, requiring long switching times, so we did not consider it further. The phase noise after scaling by r is about equal for 15 and 43 GHz, and although the switching time from 43 to 86 GHz is shorter, we preferred the higher detection SNR at 15 GHz.

ν GHz	θ deg	SEFD Jy	S mJy	SNR	r	noise deg
15	42	550	169	7.8	5.61	41.2
22	102	888	182	5.2	3.88	42.8
43	25	1436	208	3.7	2.00	31.0

Table 1. Possible reference frequencies, the angular separations of their feed horns from the 86 GHz horn, SEFDs, the expected M81 flux density as calculated from an estimated 150 mJy at 8.4 GHz (Bietenholz et al. 2000) and assuming a spectral index of $\alpha = 0.2$ (Reuter & Lesch 1996), the expected SNR in a 10 s observation, the frequency ratio to 86 GHz and the expected phase noise after scaling by r.

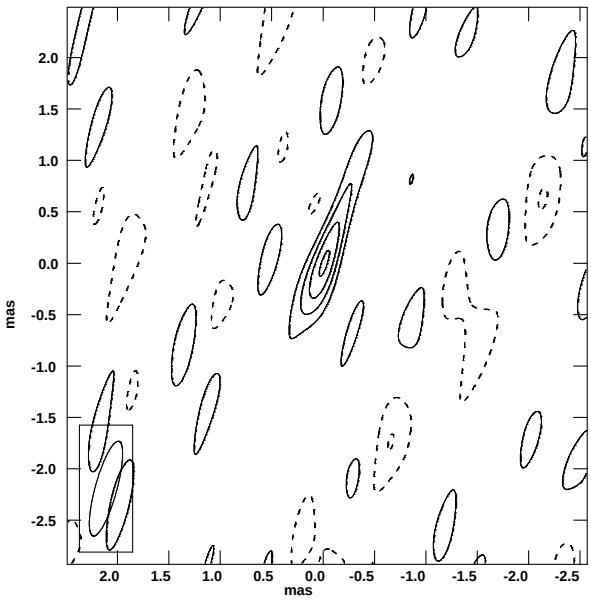

Fig. 1. 86 GHz image achieved from a 10 minute observation of 3C 279, switching between 43 and 86 GHz every 30 seconds. Self-calibration was done with a 10 minute solution interval. The peak flux density is 4.17 Jy; contours are drawn from -2 to 4 Jy in steps of 1 Jy.

3. Observations

Observations were carried out on January 5, 2002, using all antennas of the Very Long Baseline Array in excellent weather conditions at all stations, resulting in atmospheric coherence times of more than 100 s at 86 GHz. We observed 3C 279 and M81 using all possible frequency pairs of 15, 43 and 86 GHz, although we did not equally distribute the observing time among those pairs. M81 was predominantly observed switching between 15 and 86 GHz because it is at the limit for self-calibration at 43 GHz. The cycle times on 3C 279 varied from 30 s (15 s at each frequency) to 90 s, and the cycle times on M81 were 30 s throughout.

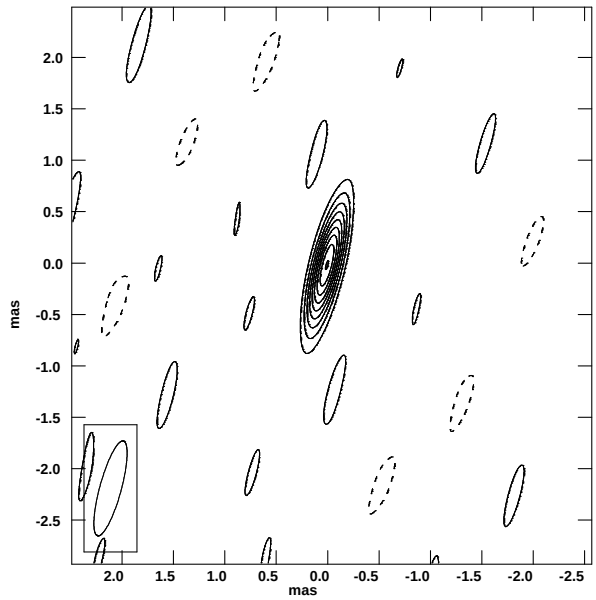

Fig. 2. The same data as in Fig. 1, but self-calibration was done at 43 GHz and the phase solutions were multiplied by r and transferred to the 86 GHz data. The peak flux density has increased to 9.07 Jy; contours are drawn from -2 to 9 Jy in steps of 1 Jy.

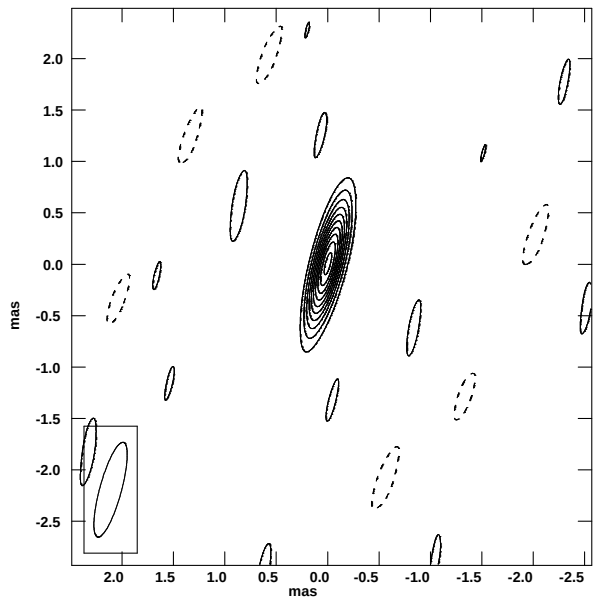

Fig. 3. The same data again, but phases were determined using self-calibration at 86 GHz with a solution interval of 30 s, equal to the scan length. The peak flux density is now 10.4 Jy; contours are drawn from -2 to 10 Jy in steps of 1 Jy

4. Data Reduction

Data reduction was carried out in Bonn, Germany and in Socorro, USA to exchange experience with the NRAO staff. After loading the data into AIPS, the 3C 279 data were inspected to develop a flagging scheme based on the

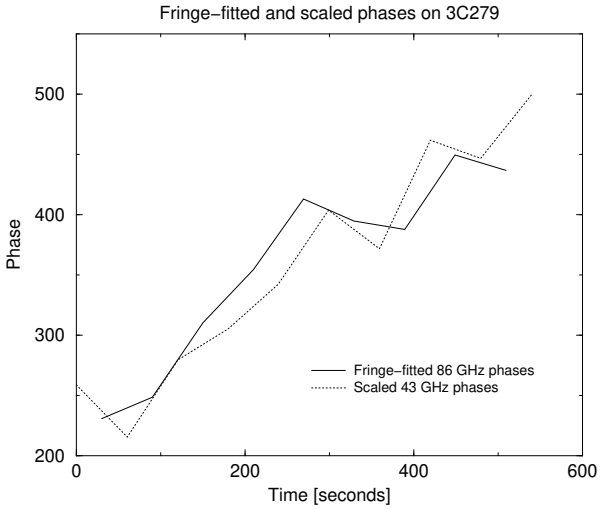

Fig. 4. Comparison of the 86 GHz phases (solid line) and the scaled 43 GHz phases (dotted line) on the LA-NL baseline. After phase wraps have been taken out, the scaled 43 GHz phases follow the 86 GHz phases remarkably well.

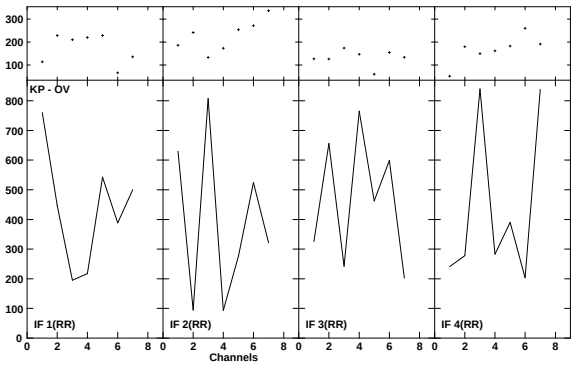

Fig. 5. Sample detection of M81 on a short baseline (Kitt Peak to Owens Valley) in 20 minutes of data. The top panel shows the phase of the vector-averaged cross-power spectrum in degrees, the lower panel the amplitude in mJy. Eight channels in each IF have been averaged for this figure.

frequency switching times. We found that the first 6 to 7 s of each scan needed flagging, independent of $\nu_{\rm ref}$. We noticed that the sub-reflectors do not always come into position, resulting in pure noise during the affected scans. The flagging tables generated by the online systems keep track of those events. We have merged the online flagging tables with our flagging scheme for optimal performance. The data were amplitude calibrated using $T_{\rm sys}$ and gain measurements. Fringe-fitting on 3C 279 was performed at each frequency on a short section of good data at all antennas to compensate for single-band delays and intra-IF phase offsets. This allowed averaging across the band during self-calibration in the later stages of data reduction.

4.1. 3C 279

We developed the calibration strategy using 10 minutes of data switching between 43 and 86 GHz (frequency ratio $r = 2.00$) every 30 s on 3C 279. Self-calibration was used to determine the phase solutions at 43 GHz. The solutions were exported to a plain text file and read into a Python program to multiply the phase solutions by r and reformat the data suitable for reading into AIPS. From each two adjacent solutions, we calculated the phase rate to allow interpolation in AIPS. Although for this special frequency pair, r is exactly 2 by good fortune, we soon discovered that the non-integer frequency ratio $r = 5.61$ chosen for the bulk of our M81 observations caused unpredictable phase jumps after multiplying the phase solutions by r. This can be understood if one pictures a time series of phase solutions at $\nu_{\rm ref}$, where the phase undergoes a 360° turn between two adjacent scans. This turn of phase will have no effect at $\nu_{\rm ref}$, but in case r is a non-integer, the phase at $\nu_{\rm t}$ will show a step, because $\phi_{\rm ref} \times r \bmod 360 \neq 0$. The problem can only be solved if one keeps track of all phase turns at $\nu_{\rm ref}$ over the whole observing run. We therefore implemented data plotting and interactive solution editing in our software to remove or introduce turns of phase in the phase-time series where it seemed obvious. After scaling the solutions by r, the calibrated visibility phases were constant with time, but an instrumental antenna-based offset remained. We measured this offset using self-calibration with a solution interval equal to the length of the observation, in this case 10 minutes. After this final step, the data were imaged.

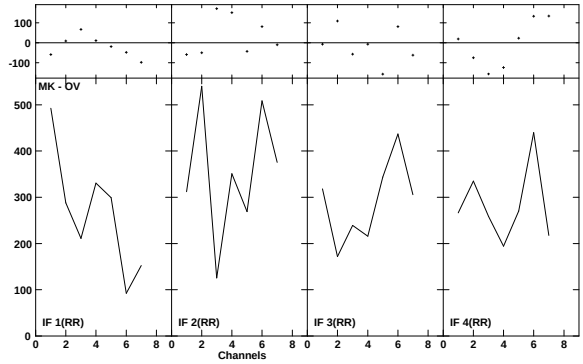

Fig. 6. Sample detection of M81 on a long baseline (Mauna Kea to Owens Valley) within 20 minutes of data. Axis are the same as in Fig. 5.

The gain in image quality is illustrated in Fig. 1-3. Fig. 1 shows the data after self-calibration with a solution interval of 10 minutes. This has brought the visibility phases to zero on average, but the loss due to atmospheric fluctuations is significant. Fast frequency switching (Fig. 2) yields an image that shows 90 % of the flux density shown in Fig. 3, which has been self-calibrated at 86 GHz. Thus, the coherence loss is only 10 %. Fig. 4 shows the phase solutions obtained via self-calibration at $\nu_{\rm t}$ and those obtained via self-calibration at $\nu_{\rm ref}$.

4.2. M81

The data reduction was done in the same way as for 3C 279, and self-calibration with a solution interval of 15 s at 15 GHz yielded about 97 % good solutions. Due to the non-integer frequency ratios, it was not possible to integrate longer than 35 min, the longest continuous time spent cycling between 15 and 86 GHz. Also, only 8 s out of 30 s delivered good data because we mostly used a short symmetric cycle time, so the sensitivity was not sufficient after 35 min (i.e. only 9 min of good data at 86 GHz) to determine the phase offset between 15 and 86 GHz. As a consequence, we were not able to image M81 and we only made marginal detections in data plots. (Fig. 5 and 6).

However, this result is preliminary, and more work is in progress. We plan to use more sophisticated methods in determining phase solutions at $\nu_{\rm ref}$, e.g. to consider the ionosphere's electron content, to estimate the tropospheric delay and to use polynomial fits to the phase-time series for better interpolation results. Every single aspect will only have little effect, but together, they might yield more reliable phase solutions at 86 GHz.

5. Conclusions

We have developed a new phase-referencing strategy to make mm-VLBI observations of sources too weak for self-calibration. The strategy is based on rapid changes between the target frequency and a reference frequency and uses scaled-up reference frequency phase solutions to calibrate the target frequency. We have observed 3C 279 as a strong test source and M81 as a weak science target. Using this technique, we were able to image 3C 279 at 86 GHz with a 10 % coherence loss compared to conventional self-calibration, and, for the first time, we were able to make a marginal detection of M81 at 86 GHz.

We have learnt three basic lessons from our project: 1) To prevent loss of coherence occuring from phase wraps at $\nu_{\rm ref}$, one should select frequencies such that their ratio is an integer. Given the VLBA frequency agility, one can almost always tune the frequencies to satisfy this condition. 2) To increase efficiency, one should use asymmetric switching times. The symmetric times that we used gave us only 8 s, or 25 % of data per cycle of 30 s duration. For future projects, we will use cycles of 60 s with 16 s at $\nu_{\rm ref}$, 7 s for switching, 30 s at $\nu_{\rm t}$ and 7 s for switching back to $\nu_{\rm ref}$. This is only possible in good weather conditions, when the atmospheric coherence time is 60 s or longer, but the VLBA's dynamic scheduling ensures a high probability. 3) One should use regular scans on a strong calibrator to monitor the phase offset between the frequencies of interest.

Fast frequency switching turns out to be a powerful tool for highest resolution VLBA images of weak sources. In some of the nearest, but unfortunately radio-weak AGNs, it might reveal the jet collimation region on scales of tens of Schwarzschild radii. However, it can also be used at lower frequencies, e.g. to phase-reference 15 GHz observations using interleaved 5 GHz scans. Atmospheric coherence and frequency switching times should be less problematic at these frequencies.

Fast frequency switching is basically a phase referencing technique, so it will reference the $\nu_{\rm t}$ data to the core position at $\nu_{\rm ref}$. After phase transfer, the $\nu_{\rm t}$ phase on a given baseline will contain a time-dependent offset which comprises the sum of a constant instrumental term, $\Delta\Phi_{\rm instr}$, and a term due to the source geometry at $\nu_{\rm t}$, $\Delta\Phi_{\rm geo}$. If the core at $\nu_{\rm t}$ is shifted with respect to the $\nu_{\rm ref}$ core, $\Delta\Phi_{\rm geo}$ will be a sinusoid whose period is 24 h, whose amplitude is a measure for the core shift between the two frequencies and whose zeros give the direction of the shift. $\Delta\Phi_{\rm instr}$ and $\Delta\Phi_{\rm geo}$ can be separated by monitoring $\Delta\Phi_{\rm instr}$ on a calibrator and fitting a sinusoid to the residual phase solutions on the source.

Using this technique, it should be possible to look for core shifts due to optical depth effects in radio jets, because the bulk of emission in jets comes from the $\tau = 1$ surface, and this surface is expected to move closer to the central mass when higher frequencies are observed. In low-luminosity AGNs like Sgr A* and M81, two emission models have been suggested, using either scaled-down jets like in quasars (Falcke et al. 1993), or spherical advection-dominated accretion flows (ADAFs; Rees 1982; Melia 1994; Narayan et al. 1995). These models can be distinguished because only the jet-like emission should have a core shift, and we have proposed to look for it in Sgr A* and M81 using a variety of frequencies.

Acknowledgements. The VLBA is an instrument of the National Radio Astronomy Observatory, a facility of the National Science Foundation, operated under cooperative agreement by Associated Universities, Inc. E.M. acknowledges partial support from the EC ICN RadioNET (Contract No. HPRI-CT-1999-40003).

References

Appl, S. & Camenzind, M. 1993, A&A, 270, 71
Falcke, H., Mannheim, K., & Biermann, P. L. 1993, A&A, 278, L1
Junor, W., Biretta, J. A., & Livio, M. 1999, Nature, 401, 891
Koide, S., Meier, D. L., Shibata, K., & Kudoh, T. 2000, ApJ, 536, 668
Melia, F. 1994, ApJ, 426, 577
Narayan, R., Yi, I., & Mahadevan, R. 1995, Nature, 374, 623
Rees, M. 1982, in: The Galactic Center, AIP Conf. 83, eds. Riegler & Blandford, p. 166